Geomorphology 253 (2016) 289–304

Contents lists available at ScienceDirect

Geomorphology

journal homepage: www.elsevier.com/locate/geomorph

Aggradation–incision transition in arid environments at the end of the Pleistocene: An example from the Negev Highlands, southern Israel

Galina Faershtein [a,b,*], Naomi Porat [a], Yoav Avni [a], Ari Matmon [b]

[a] Geological Survey of Israel, 30 Malkhe Israel St., Jerusalem 95501, Israel
[b] Institute of Earth Sciences, The Hebrew University of Jerusalem, Jerusalem 91904,Israel

ARTICLE INFO

Article history:
Received 3 March 2015
Received in revised form 21 October 2015
Accepted 24 October 2015
Available online 26 October 2015

Keywords:
Incision
Negev Highlands
Israel
Loess sediments
OSL dating

ABSTRACT

One of the most significant environmental processes that occurred at the transition from the last glacial phase into the present inter-glacial phase in arid regions was the shift from aggradation to incision in the drainage systems. This is evident by the sharp transition from a fluvial regime depositing fine-grained sediment within the wadis to intensive incision which formed gullies and narrow channels that dissected the late Pleistocene sediments. In order to investigate this transition, we studied three small-scale basins in the arid region of the Negev Highlands, southern Israel. Although the selected basins drain toward different base levels, their geomorphological parameters, particle size distribution of alluvial units and their OSL ages are similar. Sediments from the penultimate glacial cycle are found in patches in the bigger catchments. Fluvial loess was widely deposited since at least 67 ka until after 28 ka, covering valleys and slopes. Between ~28 and ~24 ka, loess was washed from the slopes into the channels, exposing the underlying colluvium. At ~24 ka erosion began with the transport of slope colluvium as gravels into the valleys that eroded the underlying loess sediments. Incision became dominant at ~12 ka and is still ongoing and intensifying. Dust and reworked loess continued to be deposited during the main incision stages. It is proposed that the transition from aggradation to incision was controlled by rates of loess supply and removal. Until ~24 ka dust choked the drainage system and only after reduction in dust supply was erosion and incision possible. It began first on the slopes and then in the channels. Our results show that an increase in precipitation is not a prerequisite for initiation of incision as is often assumed. Similar processes are described in other arid zones around the world.

1. Introduction

In arid and semi-arid environments, such as the Middle East, Australia, and Inner Mongolia (China), aggradation of alluvial sediments during the last glacial cycle is well-documented (e.g., Williams et al., 2001; Avni et al., 2006, 2010; Haberlah et al., 2010). Most of these sediments originated from aeolian desert dust, accumulating as fine-grained loess sediments combined with clasts originating from the local geological units (Avni et al., 2006). The pattern of aggradation gave way to erosion and incision which continues to the present. This shift in the deposition/erosion sediment budget can be seen in arid and semi-arid environments worldwide (e.g., Botha et al., 1994; Eitel et al., 2001; Waters and Haynes, 2001; Williams et al., 2001; Avni et al., 2006, 2010; Walker and Fattahi, 2011). In some regions this happened toward the last glacial maximum (LGM, 24–18 ka; Mix et al., 2001; e.g., Haberlah et al., 2010; Avni et al., 2012), while in others it happened later in the early Holocene (~9 ka; e.g., Waters and Haynes, 2001; Avni et al., 2010; Walker and Fattahi, 2011).

Previous studies that investigated the late Pleistocene transition from aggradation to incision were mostly conducted in large drainage basins in several regions of both hemispheres: in the northern hemisphere at the northern edge of the Sahara Desert in Israel and Sinai (Ben-David, 2003), at the edge of the Gobi Desert (Avni et al., 2010), southwest USA (Waters, 1988; Bull, 1997; Waters and Haynes, 2001), and at several sites in eastern Iran (Walker and Fattahi, 2011 and references therein). In the southern hemisphere the shift from aggradation to incision was documented in Kwa-Zulu Natal in South Africa (Botha et al., 1994; Clarke et al., 2003), northern Namibia (Eitel et al., 2001), and South Australia (Williams et al., 2001; Haberlah et al., 2010). Most of those studies used optically stimulated luminescence (OSL) or ^{14}C as the main dating tool, and determined the timing of this transition mostly to 18–9 ka. The different researchers suggest general climate changes as responsible to the aggradation/incision transition. For example, increase in precipitation (Eitel et al., 2001, 2006; Walker and

* Corresponding author at: Geological Survey of Israel, 30 Malkhe Israel St., Jerusalem 95501, Israel.
E-mail address: galaf@gsi.gov.il (G. Faershtein).

http://dx.doi.org/10.1016/j.geomorph.2015.10.017
0169-555X/

Fattahi, 2011) or, in contrast, desertification (e.g. Avni et al., 2006). In spite of the extensive research, there are still important knowledge gaps regarding the relationship between climate changes at the end of the Pleistocene and the widespread transition from aggradation to incision at that time.

This paper presents mapping, particle size distribution (PSD) analysis, and detailed OSL chronologies of three small-scale catchments in the Negev Highlands, southern Israel. The small basins best record the initiation of incision. Based on the morphological similarity between the basins and the sedimentological characteristics and ages of their alluvial

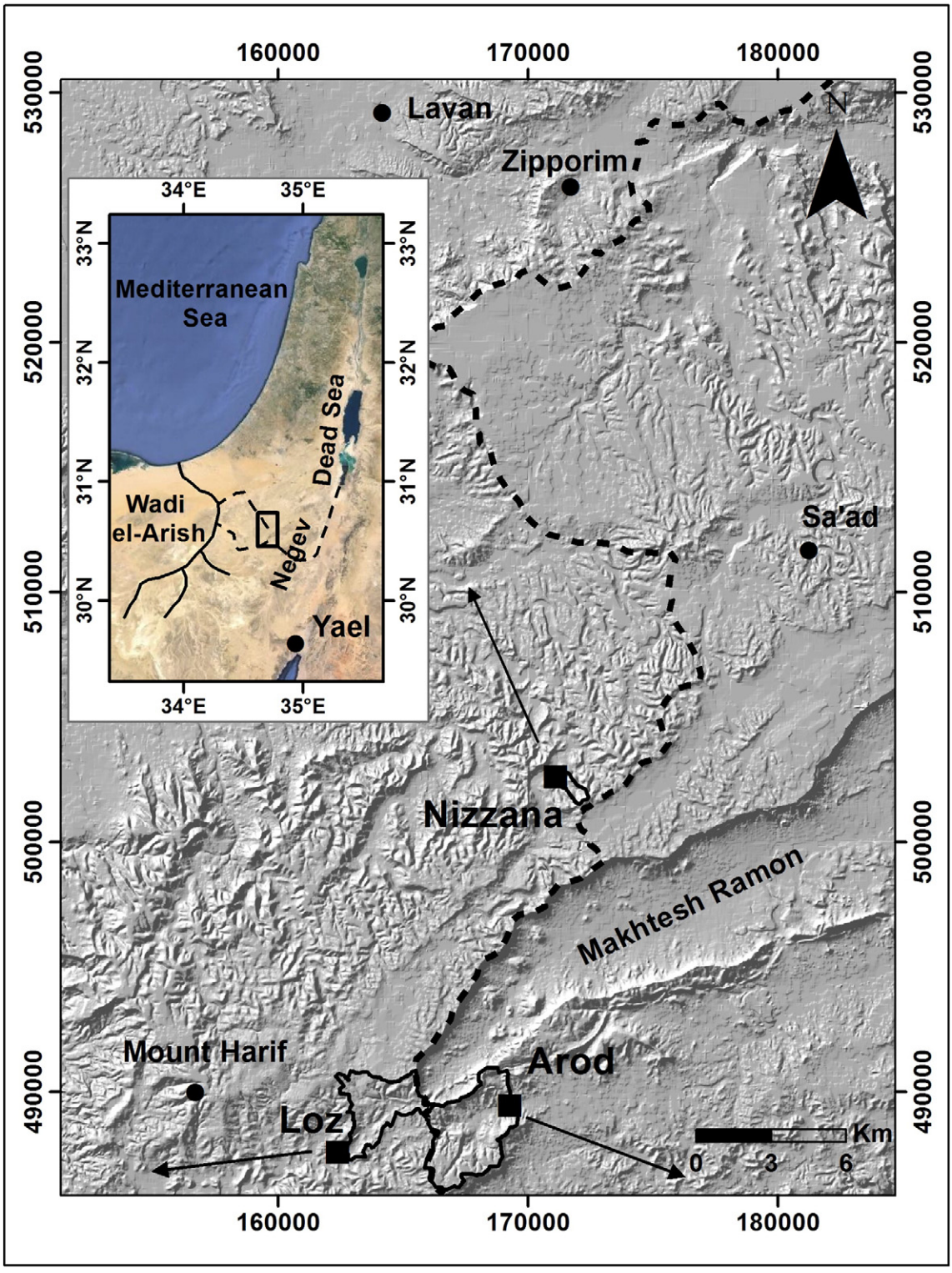

Fig. 1. Location map of the study sites within the Negev Highlands. Nizzana, Loz, and Arod sites are marked as squares. The catchments up to the study sites are marked. Previously studied areas are marked with a circle (Avni et al., 2006, 2012; Crouvi et al., 2008; Enzel et al., 2012). Arrows mark the general drainage direction. The thick dashed line shows the main water divide (DEM from Hall, 1997; ITM coordinate system). Inset — Location map of the Negev Highlands (marked in rectangle). The channels from the study sites to their base levels are marked with dashed lines. (Image from Google Earth 7.12.2041. "East Mediterranean", 31.395297N, 34.652278E, Image Landsat, 4/10/2013, February 18 2015.)

units, we aim to reconstruct the chain of events that caused the shift from aggradation to incision at the end of the Pleistocene, to investigate the transition itself, and to place those events in a narrow time frame.

1.1. Research area

The relatively high area of the central Negev (260 km^2; 600–1000 m above sea level), is known as the Negev Highlands (Fig. 1). Bedrock consists of marine sedimentary rocks, mainly limestone, dolomite, chalk, and chert of Upper Cretaceous to Tertiary age (Avni, 1991; Zilberman, 1991). The present landscape has evolved since the late Miocene–early Pliocene, when the Negev Highlands were tectonically uplifted and tilted to the east toward the embryonic Dead Sea rift (Avni, 1991). During the early Pleistocene the region was uplifted to its final elevation.

The Negev Highlands drain into two regional drainage basins, the Mediterranean Sea in the northwest and the Dead Sea in the northeast (Fig. 1). The drainage system has developed during the Pleistocene through several phases of aggradation and incision, which left a series of alluvial terraces along the valleys (Zilberman, 1991). During the middle to late Pleistocene, several meters of aeolian loess were deposited throughout the central and northern Negev (Yaalon and Dan, 1974). Only small relics of this loess cover are preserved, mostly on high plateaus such as Mt. Harif, where its thickness reaches 4 m (Crouvi et al., 2008). Most of this loess was eroded and redeposited along the drainage systems as valley fill, with a thickness of up to 15 m in the central Negev and up to 20 m at the northern Negev (Avni, 1991; Zilberman, 1991). Presently, the stream channels cut through this alluvial fill, exposing bedrock in many wadis (ephemeral streams).

1.2. Climate

The Negev Highlands are located at the northeastern margins of the Sahara desert belt. Average annual temperature ranges between 17 and 19 °C, depending on elevation, and annual precipitation ranges between 70 to 100 mm. Precipitation falls mostly during the winter months (December to February), and is the result of low intensity rainstorms originating in the Mediterranean Sea and lasting several hours (Sharon, 1972; Sharon and Kutiel, 1986). Rare autumn and spring intense storms, originating in the Red Sea and bringing air masses from the equator (Kahana et al., 2002; Tsvieli and Zangvil, 2007) result in powerful, short rains.

Floods in the region are usually formed as a result of rare, high precipitation events from well-developed Mediterranean cyclones accompanied by pronounced upper-level troughs (Kahana et al., 2002). Rainstorms from the Red Sea can also cause floods. Although most rain water infiltrates through the valley fill, occasionally floods develop and in most cases reach the drainage base level (Yair, 1983). In general, a 10 mm/h rain event is required to generate a flood in the region (Yair and Kossovsky, 2002), although different intensities of precipitation are required on rocky vs. soil-covered slopes.

1.3. Previous research

Loess sediments are an abundant feature in the northern Negev and the Negev Highlands (Yaalon and Dan, 1974; Crouvi et al., 2009). They were extensively studied and used for constructing the paleoclimate of the late Pleistocene in the area (e.g. Horowitz, 1979; Bruins and Yaalon, 1979; Issar and Bruins, 1983; Gerson and Amit, 1987), and were interpreted as indicating a wetter environment during the loess deposition phase. A series of studies investigated infiltration and runoff generation on rocky vs. loess-covered slopes in the northern Negev and Negev Highlands (Yair, 1983, 1987; Yair and Lavee, 1985). Their results showed that the studied rocky slopes produce significantly more runoff than those covered by loess. This brought Yair and Enzel (1987) to suggest that rapid accumulation of loess during the last glacial in the Negev valleys created a mantle which dramatically reduced runoff and blotted out the entire drainage network.

Previous research on the chronology of Negev loess deposition was centered in the northwestern Negev, carried out mostly over large areas, with little numerical dating (e.g. Horowitz, 1979; Issar and Bruins, 1983; Magaritz, 1986; Goodfriend and Magaritz, 1988; Zilberman, 1993; Ben-David, 2003). Ages were derived from stratigraphic relations between sedimentary units and from ^{14}C dating of archeological sites and pedogenic carbonate nodules within the loess (e.g. Issar and Bruins, 1983; Magaritz, 1986; Goodfriend and Magaritz, 1988). In general, these studies show that in the northwestern Negev loess was deposited between 70 and 10 ka by regional fluvial systems.

In recent years several studies focused on the loess sequence in the Negev Highlands using OSL dating (Avni et al., 2006, 2012; Crouvi et al., 2008, 2009; Enzel et al., 2010). Crouvi et al. (2008, 2009) investigated primary aeolian loess sequences deposited on hill tops in the Negev region. They showed that primary aeolian loess was deposited in the area almost continuously from 95 ka to 14 ka. This is in contrast to previous claims that the loess was deposited in distinct four or five pulses (Zilberman, 1991).

Avni et al. (2006, 2012) locally dated fluvial loess sequences in the Negev Highlands as part of their research of the pre-farming environment in the region. They showed that in two small basins loess deposition started prior to approximately 70 ka and ended at about 27 ka, with ensuing erosion that was expressed in the field by a gravel unit deposited on top of the loess sections, followed by significant incision. Those studies only gave a general framework to the aggradation/incision transition and did not provide details of the geomorphological processes.

2. Methods

2.1. Site selection

Three drainage basins in the Negev Highlands were selected for this study: a small tributary of Nahal Nizzana (Nizzana site), and the uppermost reaches of Nahal Loz (Loz site) and Nahal Arod (Arod site; Fig. 1; Table 1). These basins are of different sizes and drain to different base levels — Nahal Nizzana and Nahal Loz drain to the Mediterranean Sea via Wadi El Arish whereas Nahal Arod drains to the Dead Sea via Nahal Paran and Nahal Arava (Fig. 1). The three basins are of varying size, drain to different base levels, and flow along different routes. This contrast could highlight the regional driving forces on the timing of aggradation and incision, over those factors controlled by a specific base level or by single drainage basin characteristics.

2.1.1. Nizzana site

Nahal Nizzana is one of the largest catchments in the Negev Highlands and it drains the northwestern margin of Ramon anticline (Makhtesh Ramon in Fig. 1) to the Mediterranean Sea via Wadi El-Arish in Sinai (Fig. 1). The distance between the headwater of Nahal Nizzana and its outlet is 130 km. We chose a side tributary of the main Nahal Nizzana stream, located 20 km downstream from the water divide (Fig. 2). The mean elevation of the tributary is 750 m above sea level and the drainage area is 0.73 km^2. Above the confluence, Nahal Nizzana drains an area of 34 km^2. The exposed bedrock includes Turonian to Eocene carbonates and Senonian chalk and chert.

2.1.2. Loz site

Nahal Loz drains the western end of the Ramon anticline into the Mediterranean Sea via Wadi El Arish along a route of 150 km. The study site is located at the uppermost reaches of Nahal Loz (Fig. 1). Upstream of the study area, Nahal Loz drains 6 km^2 at an average elevation of 900 m. The exposed bedrock is composed of Lower Cretaceous to Middle Eocene carbonates and chert.

Table 1
Basin characteristics of the study sites.

Site	Drainage basin area [km^2]	Base level	Distance to base level [km]
Tributary of Nahal Nizzana	0.7	Mediterranean sea	130
Nahal Loz	6	Mediterranean sea	150
Nahal Arod	10	Dead sea	130

2.1.3. Arod site

Nahal Arod drains the southern part of the Ramon anticline through Nahal Paran to the Dead Sea, along a course of 130 km (Fig. 1). The study site is located in the upper reaches of the Arod basin, and above the study site the Arod basin drains 10 km^2 at an average elevation of 850 m. At the site, bedrock is composed of Santonian chalk. However, a large variety of rock unites ranging in age from the upper Cretaceous to middle Eocene are exposed throughout the drainage basin.

2.2. Field work

Morphostratigraphic mapping of the study sites was carried out using aerial photos complemented by detailed ground survey. The morphostratigraphic units were identified based on their relative height above the present-day active channel and their sedimentological characteristics. Stratigraphic sections within each terrace were described and measured. All stratigraphic units were sampled for PSD analysis and for OSL dating.

Samples for OSL dating were collected from selected sub-units within each of the terraces sections by drilling horizontally into the alluvial sediment. An electric spiral drill, hand augers, or trowels were used, depending on the sediment type. To prevent any exposure to light, sampling was carried out under cover and the sediments were placed immediately in light-proof bags. A complimentary sediment sample for dose rate measurements and PSD was collected from each sampling point. It should be noted that as the bedrock in the study area is mostly carbonates, the source of the quartz is entirely external (Yaalon and Dan, 1974; Crouvi et al., 2008); it has been blown in as dust during storms since the middle Pleistocene (Amit et al., 2011) and recycled by the fluvial system.

2.3. OSL dating

Twenty four sediment samples were dated using OSL, 7–9 from each basin. Sample preparation and measurements were carried out under weak orange–red light at the luminescence dating laboratory of the Geological Survey of Israel (GSI). Very fine quartz sand (88–125 μm or 74–125 μm) was extracted for OSL dating using routine laboratory procedures (Davidovich et al., 2012). Briefly, after wet sieving for the selected grain size, carbonate was dissolved using 8% HCl solution. The rinsed and dried samples were then passed through a LB-1 Frantz magnetic separator, using a current of 1.4 A on the magnet, to remove heavy minerals and most feldspars (Porat, 2006). Etching in concentrated (40%)

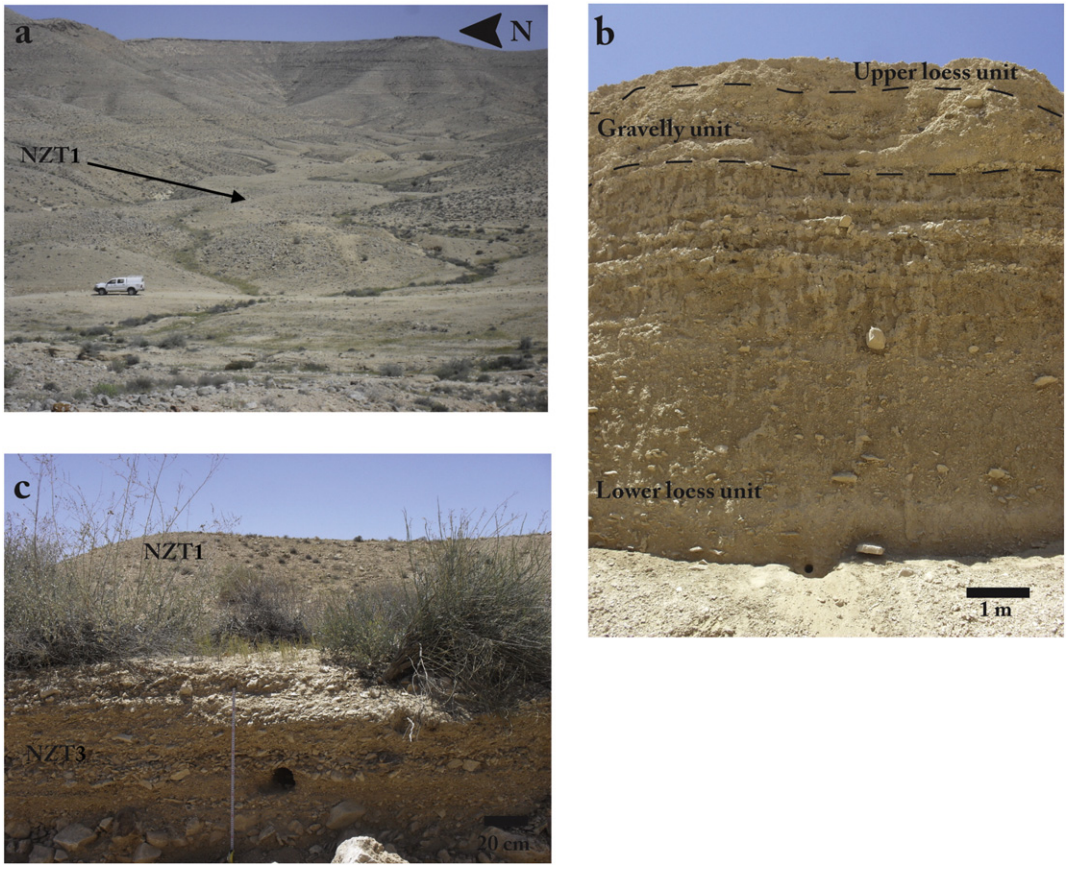

Fig. 2. The Nizzana site. a. A view of the small tributary outlet taken from the opposite bank of the main Nahal Nizzana. The main surface in the center of the basin is terrace NZT1. b. Exposed section (section B in Fig. 4b) of terrace NZT1, showing the three main sedimentary units. c. Exposed section (section D in Fig. 4b) of terrace NZT3, showing mixed layers of gravels and loess. Terrace NZT1 is seen in the background.

HF for 40 min removed any remaining feldspars and the outer 20 μm of the individual quartz grains, followed by soaking in 16% HCl overnight to dissolve any fluorides which may have precipitated (Porat et al., 2015).

The purified quartz was placed on 9.8 mm aluminum discs (aliquots) using 2 mm (3 mm for very young samples) masks and silicon spray as an adhesive (~200 grains or ~400 grains for the 2 and 3 mm aliquots, respectively). Equivalent dose (De) determination used a modified single aliquot regenerative (SAR) dose protocol (Murray and Wintle, 2000) that included a cleaning step of heating to 280 °C for 100 s at the end of each measurement cycle (Table S1 in supplementary data). Preheat temperatures were selected according to dose recovery tests over a range of temperatures carried out on selected samples from each site (Fig. 3a). These showed that a recovery of 94–100% is achieved using a pre-heat of 10 s at 260 °C, a test dose of ~9 Gy and a test dose pre-heat of 5 s at 200 °C (240 °C for Loz site). All luminescence measurements were undertaken using TL/OSL DA-12 or DA-20 readers (Bøtter-Jensen and Murray, 1999), equipped with blue LEDs (Thomsen et al., 2006). Single grain (SG) OSL measurements used a focused green (532 nm) laser (Bøtter-Jensen et al., 2000). Irradiation was by a calibrated ^{90}Sr β source, and the luminescence signal was detected through 7 mm U-340 filters. Eighteen to thirty six aliquots were measured for each sample. After distinct outliers were removed, the central age model (CAM; Galbraith and Roberts, 2012) was used to obtain a

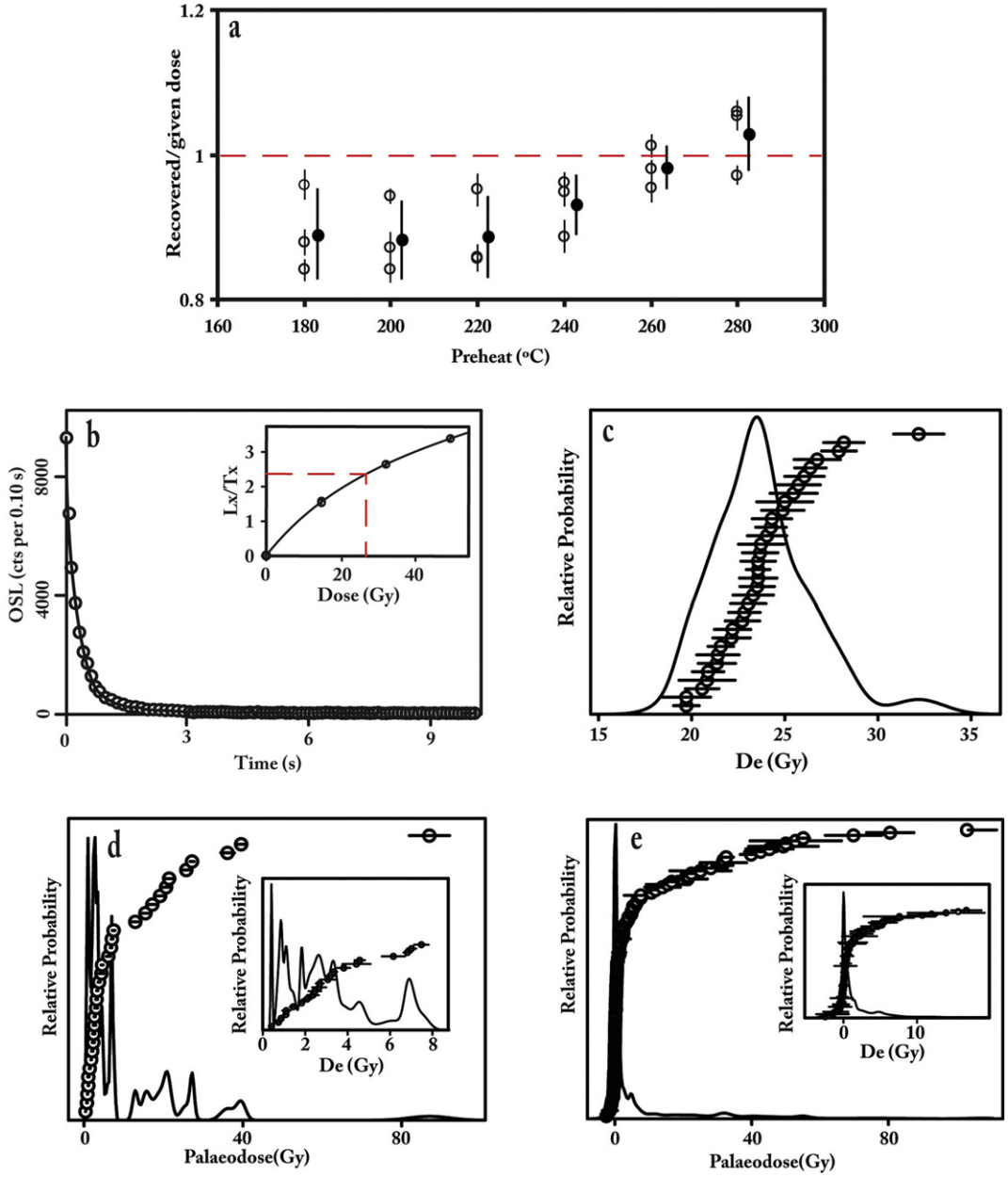

Fig. 3. OSL results. a. Dose recovery over a range of pre-heat temperatures for sample FGA-1. Test dose (TD) preheat was at 20 °C below pre-heat temperature in all cases. Dose recovery of over 95% is achieved using pre-heat temperature of 260 °C and TD pre-heat of 240 °C. Individual aliquots are shown as open circles and averages with errors as full circles. b. The first 10 s of the natural OSL signal (measured for 40 s) of one aliquot from sample FGA-26. De = 26 Gy. The signal decays to less than 1% within 2 s. Inset - Dose response curve for the same aliquot. Three dose points overlap at 15 Gy (two recycling points and one IR depletion point). c. A probability density function plot for sample FGA-26 with individual De values and errors. De = 24 ± 1 Gy, calculated with the CAM. A normal distribution with over-dispersion (OD) of 10% is typical of the loess units, indicating adequate bleaching. d. A probability density function plot of 2 mm aliquots measured for sample FGA-25. The CAM De is 2.0 ± 0.3 Gy. The positively-skewed distribution with OD of 100% is typical of the poorly bleached gravel units. Inset — The youngest part of the distribution. e. A probability density function plot of single grain measurements for sample FGA-25. De = 0.2 ± 0.05 using the FMM. While most of the De values are close to 0, there are some values as high as 100 Gy. Inset — The youngest part of the distribution. Note the negative De values.

representative De value, with standard errors, which were propagated to the age errors.

The homogeneity of a sample is expressed by the over-dispersion (OD) parameter which represents the scatter in the De values beyond that caused by the analytical errors of single values (Galbraith and Roberts, 2012). Arnold and Roberts (2009) presented a list of published OD values and showed that the average OD of homogeneously bleached samples is 14 ± 7% for multi-grain small aliquots (up to 1000 grains) and 20 ± 9% for SG measurements. As there were usually 200 grains in each aliquot, a cut-off OD value of 20% was chosen to separate between homogeneous and heterogeneous samples.

Four heterogeneous samples were selected for SG measurements. Since quartz grain size was ~100 μm, more than one grain was present in each hole of the standard disc. Between 600 and 1200 single grain holes were measured for each sample and were screened for further data processing using the criteria suggested by Porat et al. (2009): signal intensity at least 3 times that of the background; error on the De smaller than 40% (this criteria was not applied for De values lower than 0.5 Gy); error on the test dose smaller than 30%; and recycling ratio within 20% of unity. The De values and errors were calculated using the finite mixture model (FMM) which assumes what the grain distribution consists of a number of normally distributed components (Roberts et al., 2000). The youngest component larger than 10% of all grains was selected to represent the best bleached component (Rodnight et al., 2006).

Most measurements were carried out on SG discs with standard holes (diameter and depth = 300 μm), with up to 5 grains in the upper layer of each hole. Some studies suggest that when there are multiple grains in a single hole, more than one grain contributes to the luminescence signal (Jacobs et al., 2008; Russell and Armitage, 2012) thus distorting the FMM results. To test this possible effect, one very heterogeneous sample (FGA-21) was measured using both standard SG discs and modified SG discs with smaller holes (diameter = 200 μm and depth = 150 μm), each containing 1–2 grains. Although many more grain holes were luminescent in the standard SG discs than in the modified ones (23% vs 7%), the same De value was obtained with the FMM (Table S2). These results suggest that even with regular, 300 μm holes, usually only one grain contributes to the signal; similar conclusions were recently presented by Medialdea et al. (2014). According to these results the remaining SG measurements were carried out on standard SG discs.

Five very young and heterogeneous samples, with De values up to 12 Gy, were selected for additional measurements using the standardized growth curve (SGC; Roberts and Duller, 2004). Forty-eight aliquots of 1 mm (50 grains) were measured for each sample: 5 aliquots with the full SAR protocol, in order to construct the SGC; for the remaining 43 aliquots only the natural signal, a zero dose point, and a single beta dose point were measured. Aliquots with Lx/Tx (normalized luminescence signal) of this single dose point that deviated more than 15% from that dose point in the SGC were rejected, as well as zero and negative De values. The samples' De values and errors were calculated using the FMM.

Water content was estimated at 3 ± 2% for loess samples from 0 to 1 m depth and 5 ± 2% for deeper loess samples (Crouvi et al., 2008). For samples from coarse gravel it was estimated at 2 ± 1% (Avni et al., 2006, 2012). Cosmic dose rates were evaluated using current burial depths. Dose rates of α, β and γ radiation were calculated from the concentration of the radioelements K, U and Th in the sediment, measured by ICP-MS (for U and Th) and ICP-AES (for K) with uncertainties of 3%, 5%, and 7%, respectively (Table 2).

2.4. Particle size distribution analysis

PSD analysis was carried out using Malvern MS-2000 laser diffraction analyzer. Measurement procedure included: hand sieving and separation of the <2 mm size fraction, dissolving of organic matter in 8% H_2O_2 for 3 days, stirring for 5 min in 40 ml of distilled water with 3 drops of sodium hexametaphosphate, and ultrasonication for 30 s. $CaCO_3$ was not dissolved. Three replicates of each sample were then subjected to 3 consecutive runs at a pump speed of 1850 RPM. The laser diffraction raw data was transformed into PSD using Mie scattering

Table 2
Dose rate data for the Negev Highlands OSL samples: Water contents were estimated at 3 ± 2% or 5 ± 2% for loess samples up to and below 1 m depth, respectively, and 2 ± 1% for gravel samples. Uncertainties on K, U and Th contents are 3%, 5% and 7%, respectively. Cosmic dose rates were evaluated using present day burial depths.

Sample	Section	Depth (m)	Grain size (μm)	Water contents (%)	K (%)	U (ppm)	Th (ppm)	Ext. α (μGy/a)	Ext. β (μGy/a)	Ext. γ (μGy/a)	Cosmic (μGy/a)	Dose rate (μGy/a)
Nizzana												
FGA-26	A	0.4	74–125	5 ± 1	0.91	3.1	6.5	14	1172	852	219	2257 ± 56
FGA-47	A	3.2	88–125	2 ± 1	0.91	2.1	5.8	10	998	693	142	1842 ± 45
FGA-21	B	0.5	74–125	2 ± 1	0.11	1.4	1.0	5	284	230	210	730 ± 18
FGA-20	B	0.9	74–125	5 ± 1	0.91	1.8	5.2	9	975	650	187	1822 ± 45
FGA-23	B	5	74–125	5 ± 1	0.77	3.1	5.4	13	1026	752	116	1906 ± 58
FGA-22	B	8	74–125	5 ± 1	0.67	2.0	4.5	9	801	570	85	1465 ± 49
FGA-24	C	0.5	74–125	2 ± 1	0.17	1.0	1.0	4	271	197	207	678 ± 32
FGA-25	D	0.5	74–125	2 ± 1	0.13	1.7	0.9	6	331	261	210	808 ± 35
Loz												
FGA-31	A	0.2	88–125	5 ± 1	0.71	1.6	5.4	8	815	590	243	1657 ± 38
FGA-32	B	0.2	88–125	5 ± 1	0.76	2.0	6.6	10	929	701	243	1883 ± 45
FGA-30	C	1.6	74–125	5 ± 1	0.68	1.6	4.6	8	760	535	172	1475 ± 35
FGA-29	C	3.6	74–125	2 ± 1	0.12	1.3	1.2	5	280	228	135	648 ± 26
FGA-1	C	2.5	74–125	5 ± 1	0.91	2.1	5.5	10	997	681	154	1842 ± 47
FGA-48	D	1.4	88–125	5 ± 1	0.69	1.7	4.4	8	769	535	176	1487 ± 35
FGA-33	E	1.0	88–125	2 ± 1	0.78	1.9	5.1	9	905	633	185	1732 ± 39
Arod												
FGA-52	A	5.5	88–125	2 ± 1	0.30	4.8	2.0	14	839	669	110	1632 ± 49
FGA-40	B	0.2	88–125	5 ± 1	0.51	3.3	4.0	12	862	665	243	1782 ± 45
FGA-34	C	5.2	88–125	5 ± 1	0.34	6.7	1.7	19	1097	871	113	2010 ± 79
FGA-37	D	0.2	88–125	5 ± 1	0.49	4.8	4.7	17	1056	856	243	2172 ± 56
FGA-38	D	0.15	88–125	5 ± 1	0.34	3.9	2.7	13	792	630	253	1687 ± 44
FGA-36	E	2.5	74–125	2 ± 1	0.06	6.2	0.6	18	846	719	154	1738 ± 61
FGA-51	E	2.4	88–125	5 ± 1	0.47	3.8	2.8	12	846	639	156	1653 ± 43
FGA-50	F	1.4	88–125	5 ± 1	0.53	5.6	3.6	18	1133	884	176	2211 ± 64
FGA-39	G	0.8	74–125	2 ± 1	0.32	7.7	1.6	24	1254	1001	190	2469 ± 74

model, with optical parameters of RI = 0.52 and A = 0.1 (Eshel et al., 2004). The data were also converted to the broad categories of gravels (>2 mm), sand (0.063–2 mm), and fines (<0.063 mm).

3. Results

3.1. OSL ages

The OSL ages range from 148 ± 12 ka to 0.2 ± 0.05 ka (Table 3). At all sites, the ages are in stratigraphic order and, in general, similar units from different sites have similar ages. The luminescence signal of all samples is dominated by the fast component, and decays to less than 1% in 2 s (Fig. 3b). Regarding quality assurance, all samples showed recycling ratios within 5% of unity (Fig. 3b), a recuperation of less than 2% of the Ln/Tn, and negligible feldspar contamination as measured by the IR depletion ratio (Duller, 2003).

The distribution of the De values of most samples from the fluvial loess units is normal or close to normal (Fig. 3c), with OD values lower than 20%, indicating a homogeneously bleached population of grains (Arnold and Roberts, 2009). The De distribution of samples from coarse gravel units is usually positively skewed (Fig. 3d), with scatter greater than 50%, indicating a heterogeneous grain population most likely due to partial bleaching during transport (Olley et al., 2004). The OD values of those samples range between 19% and 100%. In general, the larger the catchment the smaller is the OD value, reflecting the longer transport distance and better bleaching.

As expected, FMM ages of SG and 1-mm aliquots measured using the SGC, are younger than the 2-mm aliquot ages (Tables 3, S2 and S3), as the first two techniques enabled the isolation of the youngest grain population which was fully bleached during the last sedimentation cycle. Interestingly, all samples had some grains with very high De values, corresponding to ages over 100 ka (Fig. 3e).

3.2. Morphology and morphostratigraphy

3.2.1. Nizzana site

Three fluvial terraces were mapped at this site (Fig. 4a). The limestone bedrock is exposed only at the upper part of the stream, while down-stream the base of the fluvial section is not exposed. The highest, main terrace NZT1, is 8–9 m high and is found along the entire channel length. It comprises 3 units separated by unconformities. The lower unit, 5–7 m thick, is composed of fluvially reworked loess sediment with carbonate nodules, gastropod fragments and rootlets. Gravel lenses and layers 10–20 cm thick are mostly located at the bottom and the top parts of this unit. The exposed base of the unit was dated to 67 ± 4 ka while its upper part was dated to 28 ± 1 ka (Fig. 4b). The middle unit is 0.5–2 m-thick gravel that truncates the lower unit at different levels, filling erosive channels, reaching its maximum thickness where sediment flow is concentrated on the slopes. The unit is composed of gravels, about 90% of which are smaller than 1 cm, the rest reaching up to 30 cm. Fine gravel, combined with re-deposited loess, form elongated lenses. In some places poorly developed bedding is identified. This gravel unit was dated from 20 ± 1 ka to 8 ± 1 ka. The upper unit is gravel-free loess, 0.2–1 m thick (Fig. 2); its upper part was dated to 10.5 ± 0.3 ka (Fig. 4b).

Table 3
OSL data and ages for the Negev Highlands samples. The central age model (CAM) was used to obtain representative De values, with standard errors propagated to the age errors. Single grain (SG) and 1 mm aliquots (measured using the SGC) De values and errors were calculated using the youngest component greater than 10% obtained from the Finite Mixture Model (FMM). No. of aliquots — the number of aliquots or grains accepted for De determination out of those measured. OD — over-dispersion. Final ages are in bold. Figs. 4–6 show ages on respective sections.

Sample	Section	Location	Depth (m)	No. of aliquots	OD (%)	De (Gy)	Dose rate (μGy/a)	Age (ka)
Nizzana								
FGA-26	A	Terrace NZT1 — upper loess unit	0.4	33/33	10	24 ± 1	2257 ± 56	**10.5 ± 0.3**
FGA-47	A	Terrace NZT1 — middle of the gravelly unit	3.2	22/24	34	36 ± 2	1842 ± 45	**20 ± 1**
FGA-21	B	Terrace NZT1 — base of the gravelly unit	0.5	31/32	36	18 ± 1	730 ± 18	24 ± 2
SG				208/900	72	6 ± 1		**8 ± 1**
FGA-20	B	Terrace NZT1 — top of the lower loess unit	0.9	34/34	18	52 ± 2	1822 ± 45	**28 ± 1**
FGA-23	B	Terrace NZT1 — middle of the lower loess unit	5	33/33	15	64 ± 2	1906 ± 58	**33 ± 1**
FGA-22	B	Terrace NZT1 — base of the lower loess unit	8	34/34	22	98 ± 4	1465 ± 49	**67 ± 4**
FGA-24	C	Terrace NZT2 — top	0.5	33/33	58	23 ± 2	678 ± 32	34 ± 4
SG				198/900	78	7.7 ± 0.2		**11.4 ± 0.4**
FGA-25	D	Terrace NZT3 — top	0.5	33/33	100	2.0 ± 0.3	808 ± 35	2.4 ± 0.4
SGC				39/48	100	1.05 ± 0.1		1.3 ± 0.1
SG				106/600	100	0.14 ± 0.004		**0.2 ± 0.05**
Loz								
FGA-31	A	Terrace NLZ1 — top	0.2	26/26	31	10 ± 1	1657 ± 38	6.1 ± 0.4
SGC				43/48	32	7.8 ± 0.2		**4.7 ± 0.2**
FGA-32	B	Terrace NLZ1 — top	0.2	24/24	26	12 ± 1	1883 ± 45	6.4 ± 0.4
SGC				40/48	28	8.7 ± 0.3		**4.6 ± 0.2**
FGA-30	C	Terrace NLZ2 — middle of the gravelly unit	1.6	25/25	20	15 ± 1	1475 ± 35	**10 ± 1**
FGA-29	C	Terrace NLZ2 — base of the gravelly unit	3.6	25/25	45	16 ± 2	648 ± 26	25 ± 2
SG				115/600	71	7 ± 1		**10 ± 1**
FGA-1	C	Terrace NLZ2 — top of the lower loess unit	2.5	34/36	16	64 ± 2	1842 ± 47	**35 ± 1**
FGA-48	D	Terrace NLZ2 — middle of the lower loess unit	1.4	24/24	20	63 ± 3	1487 ± 35	**41 ± 2**
FGA-33	E	Terrace NLZ3 — middle	1.0	26/26	100	2.2 ± 0.4	1732 ± 39	1.3 ± 0.3
SGC				44/48	100	0.70 ± 0.03		**0.40 ± 0.02**
Arod								
FGA-52	A	Terrace NAR1 — middle	5.5	20/20	31	241 ± 18	1632 ± 49	**148 ± 12**
FGA-40	B	Terrace NAR1 — top	0.2	25/27	29	17 ± 1	1782 ± 45	**10 ± 1**
FGA-34	C	Terrace NAR2 — base of the lower loess unit	5.2	18/18	25	133 ± 9	2010 ± 79	**63 ± 5**
FGA-37	D	Terrace NAR2 — upper loess unit	0.2	15/18	26	27 ± 1	2172 ± 56	**12 ± 1**
FGA-38	D	Terrace NAR2 — top	0.15	25/28	36	23 ± 1	1687 ± 44	**13 ± 1**
FGA-36	E	Terrace NAR2 — base of the gravelly unit	2.5	16/18	44	23 ± 1	1738 ± 61	**13 ± 1**
FGA-51	E	Terrace NAR2 — top of the lower loess unit	2.4	22/23	18	85 ± 4	1653 ± 43	**52 ± 3**
FGA-50	F	Terrace NAR2 — middle of the gravelly unit	1.4	23/24	19	52 ± 2	2211 ± 64	**24 ± 1**
FGA-39	G	Terrace NAR3 — middle	0.8	22/25	56	1.6 ± 0.1	2469 ± 74	0.6 ± 0.1
SGC				37/48	88	1.2 ± 0.1		**0.50 ± 0.04**

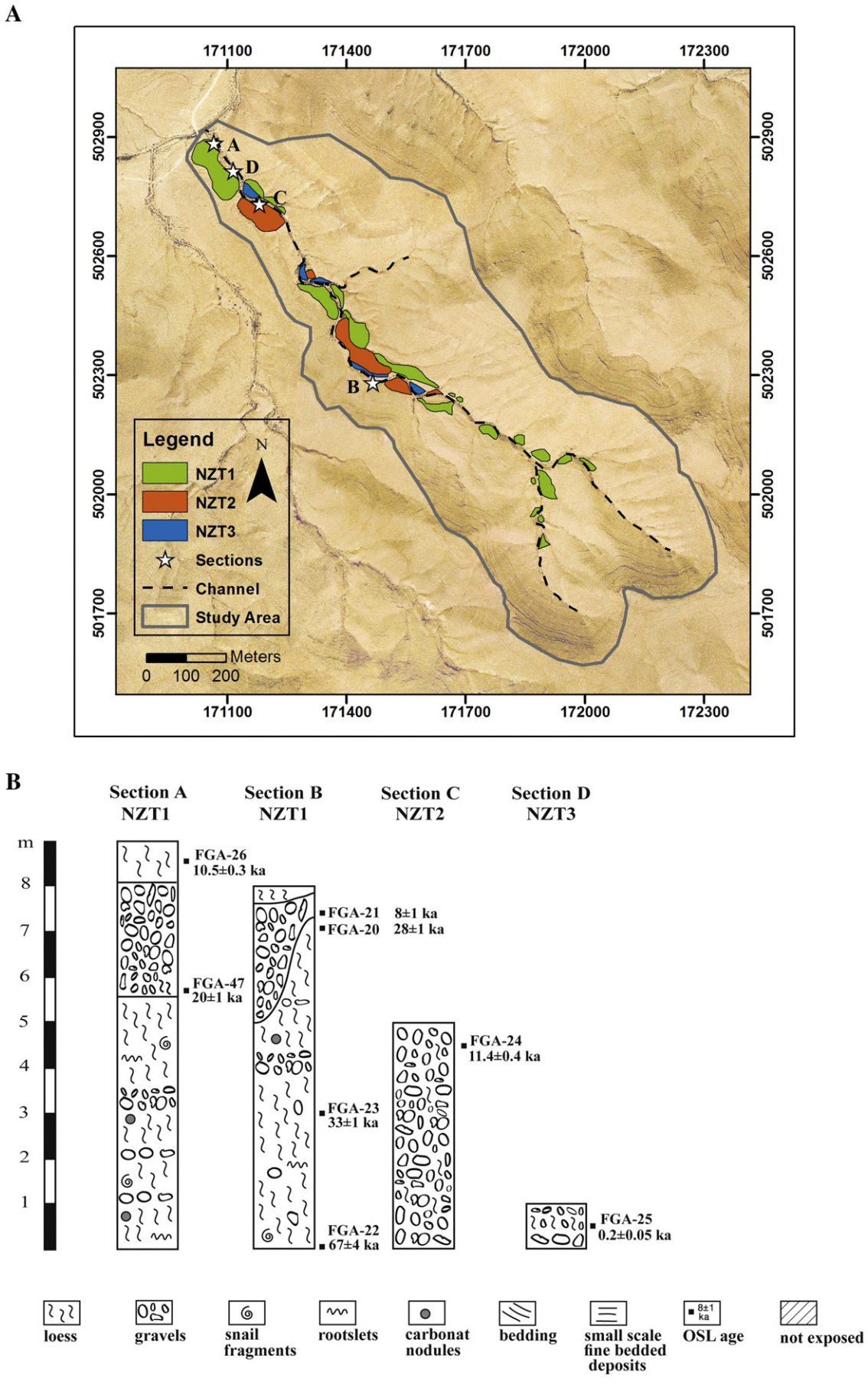

Fig. 4. a. Geomorphological map of the Nizzana site. Stratigraphic sections are marked as stars. b. Stratigraphic sections of the Nizzana site with OSL ages.

The middle terrace (NZT2) forms a distinct surface 3–5 m above the present day stream. It is composed of a mixture of gravels and fine-grained loessy sediment. A sample taken near the top of the terrace gave an age of 11.4 ± 0.4 ka. The similar appearance and age of this terrace to the gravel unit in terrace NZT1 suggests that this surface is a cut terrace inset within the older terrace. A third, lower terrace (NZT3) is only 1 m above the active channel, is composed of layered, poorly to well sorted gravel and was dated to 0.2 ± 0.02 ka.

3.2.2. Loz site

Three terraces were mapped at this site (Fig. 5a). Bedrock, mostly Coniacian fossiliferous limestone, is exposed in some places along the channel bed. The top of the upper terrace (NLZ1) is 8–10 m above the present day stream. It is located within the valley, and represents the main alluvial fill with some contribution from small side streams draining the rocky slopes on both sides of the main valley. The upper 1 m of the section is composed of loess with some gravel and its top was dated in two locations to 4.7 ± 0.2 ka. The main, second terrace (NLZ2 in Fig. 5a) is 5–6 m above the channel and comprises three units separated by unconformities. The lowest unit is 2–4 m thick, composed of prismatic fluvial loess with abundant carbonate nodules, some gastropod fragments, and rootlets. Gravels appear in thin beds in the lower part of the unit as well as dispersed throughout. This unit was dated to 41 ± 2 ka and 35 ± 1 ka (Fig. 5b). The fluvial loess is overlain by a 1–3 m-thick gravel unit, appearing in erosive channels. It can be divided into a lower bed of small (less than 2 cm in diameter), well sorted gravels, truncated by an upper bed of poorly sorted gravels with lenses of large gravels and small boulders (up to 30 cm), as well as fluvial loess lenses. Both beds were dated to 10 ± 1 ka. The gravel is covered by a 0.2–1.0 m-thick unit composed of reworked loess sediment with some gravel lenses, resembling the uppermost loess on the highest terrace NLZ1 (Fig. 5b).

Nearby within the channel there is a 5 m-deep dry well, exposing the buried fine alluvial sediments and gravel horizons located below the present active channel. In the late 80's this well was even deeper (8 m), yet bedrock was not visible (Avni, 1991), hinting at the very thick valley fill.

The top of the lowest terrace (NLZ3) is 1–2 m above the present-day stream. It is composed of two fluvial loess beds separated by an erosive unconformity expressed by a 10 cm gravel layer. The lower bed has the same characteristics as the lower fluvial loess unit in terrace NLZ2 whereas the upper sub-unit was dated to 0.40 ± 0.02 ka (Fig. 5b).

3.2.3. Arod site

Three terraces were mapped also at this site (Fig. 6a). The top of the upper surface (NAR1) is 10–12 m above the present active stream. The terrace appears as patches along the valley margins, but exposures are found only outside of the study area. Overall it is composed of mixed layers of gravels and fines. Its middle part (5.5 m below the surface) was dated to 148 ± 12 ka and its uppermost bed is reworked loess dated to 10 ± 1 ka (Fig. 6b).

The second, main terrace (NAR2) is 5–6 m high with unexposed base, and it comprises three units. The lowest unit is 2–4 m thick, consisting of fluvially deposited loess with prismatic pedogenic structures, carbonate nodules, some gastropod fragments, and rootlets. Close to the exposed base there are several gravel horizons, while in most of the unit gravels are nearly absent. At some places small scale, finely bedded lenses are seen. The exposed base was dated to 63 ± 5 ka and the top to 52 ± 3 ka (Fig. 6b). The middle unit is 2–3 m-thick gravel that truncates the lowest unit at different levels creating erosive channels. It is composed of poorly sorted gravels with lenses of better-sorted fluvial loess. Most of the fragments are gravel size, but some of them reach cobble and small boulders size. Lenses with relatively large amount of fines are present. Also, some bedding and cross-bedding are visible. The unit was dated to 24 ± 1 and 13 ± 1 ka. The upper unit is 0–1 m thick loess, with some small gravel, and was dated to 12 ± 1 ka (Fig. 6b).

The lower terrace (NAR3) is 1–2 m above the active channel. It is composed of poorly sorted gravel with some fines, and it was dated to 0.50 ± 0.04 ka (Fig. 6b).

3.3. Particle size distribution

PSD analyses show that the fraction smaller than 2000 μm both in fluvial loess and gravel units is composed mainly of coarse silt to very fine sand with a mode at 40–70 μm (Fig. 7a). The remaining grains are mostly finer with a small population at 3–10 μm and a small clay fraction. This PSD is typical for pristine loess in the Negev Highlands (Crouvi et al., 2008). The gravel units also contain a small, coarser population of 300–600 μm.

The fines (<62.5 μm) contents of the fluvial loess samples is 45–81%, and the gravel fraction (>2000 μm) of most gravel samples is over 50% (Fig. 7b). Within gravel units, embedded fine grained lenses have loess-like PSD. All samples form a mixing line between fines and gravel, with notably low sand percentage of less than 12% (except FGA-39), indicating sediment sources of both slope gravel and loess.

4. Discussion

4.1. Terraces of the Negev Highlands

The three studied sites are very similar with respect to morphostratigraphy. The main terraces at each site (NZT1, NLZ2 and NAR2) resemble each other and are constructed from the same three distinct units which have similar OSL ages. In all areas the current channel incises into this main terrace, in places exposing bedrock, and young, low gravel terraces are inset into the present channel. In the following discussion the overall history of the three sites is examined within the geomorphic and chronological framework.

4.1.1. Middle Pleistocene terraces

In the two larger basins (Loz and Arod sites) the high surface (NLZ1, NAR1) is detached from the present-day channel. At Loz only the upper 1 m is exposed and it consists of loess with some gravels. At Arod it is exposed outside the mapped area and consists of gravels and mixed layers of reworked loess and gravel. A single age of 148 ± 12 ka suggests that the sediment in this terrace was deposited during the previous glacial cycle (190–130 ka). Although the lower part of terrace NLZ1 was not dated, the similarity in the sedimentary characteristics with NAR1 and its position in the valley lead us to propose similar ages.

Additional evidence for the presence of sediments from the previous glacial cycle in the drainage basin can be found in the SG data measured for non-homogenous samples from Holocene sediments. Samples from both Nizzana and Loz sites contain grains with high De values that correspond to old ages within the previous glacial cycle. It is unlikely that the high De values of those grains result from exposure to high β dose from nearby alkali feldspars or zircon minerals (Mayya et al., 2006). The sediment is much finer (~100 μm) and with very low K contents (<0.2%) compared to the model suggested by Mayya et al. (2006), so that one can assume evenly distributed beta dose.

To better quantify this observation, each SG De value was converted to an age using the individual sample's dose rate, the ages were all combined into a single dataset (4 samples, 824 grains) and the FMM was used to isolate age components. This revealed a small population, consisting ~3% of all grains, with an average age of 145 ± 7 ka. The ubiquitous presence of such old grains in Holocene terraces implies recycling of grains from sediments deposited during the previous glacial cycle. Indeed, primary aeolian loess with suitable ages (178–134 ka) was found on Mount Harif in the Negev Highlands (Crouvi et al., 2008), supporting extensive loess deposition at the time.

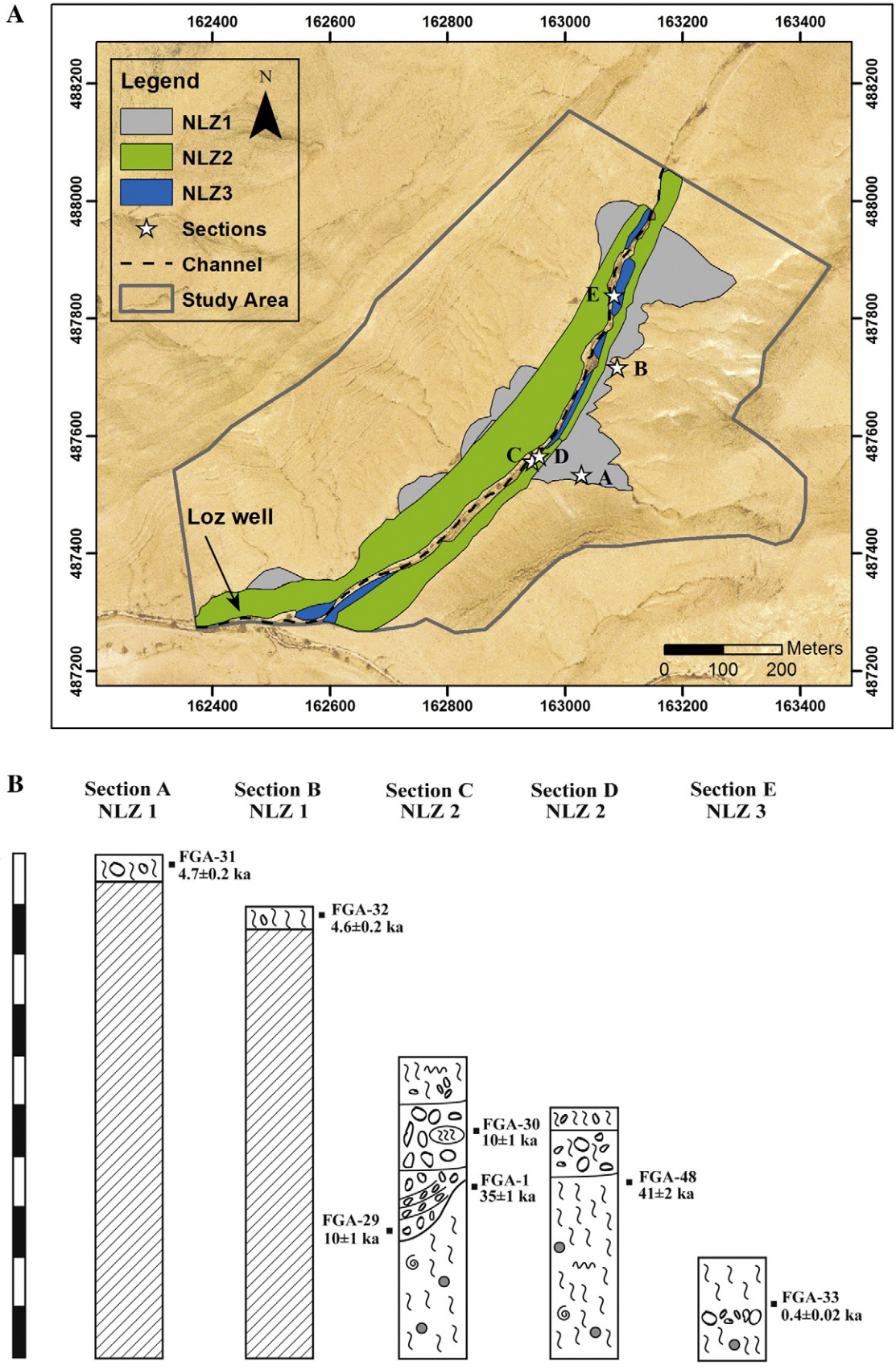

Fig. 5. a. Geomorphological map of Loz site. Stratigraphic sections are marked as stars. b. Stratigraphic sections of Loz site with OSL ages. For legend see Fig. 4b.

4.1.2. Late Pleistocene terraces

4.1.2.1. Lower fluvial loess unit. The lower fluvial loess is the oldest unit of the main terraces (NZT1, NLZ2 and NAR2) currently exposed. It is composed mostly of fluvial loess with a small proportion of gravels, with exposed thickness of about 4 m. This unit was deposited from at least ~70 ka until sometime between 28 ka to 24 ka. The OD values of most OSL samples from this unit are lower than 20%, indicating that the grains were well bleached during transport. The base of the unit is not exposed, suggesting that the onset of the deposition was before 70 ka. In all the sections, the top of the unit is truncated by the gravel unit (see Section 4.1.2.2). The fluvial loess was reworked from aeolian loess which was supplied continuously in large amounts to the region from 95 ka (Crouvi et al., 2008), and is still preserved on some slopes as "aprons" (Bowman et al., 1986). The PSD of the reworked loess is identical to that of the aeolian loess from other parts of the Negev (Crouvi et al., 2008). Similar OSL ages of 71–41 ka from fluvial loess section were reported from two other basins within the Negev Highlands by Avni et al. (2006, 2012).

4.1.2.2. Middle gravel unit. The thickness of the middle gravel unit is about 2 m. The wide range of ages, 24–8 ka, suggests that deposition was not continues, but rather in pulses which eroded the underlying fluvial loess (see Section 4.1.2.1) and deposited new sediment instead. The gravel truncates the underlying loess unit at different levels — the larger the basin the deeper the truncation: at the Nizzana site (drainage area of 0.7 km^2) the gravel eroded the fluvial loess to a level dated to 28 ± 1 ka, while at the Arod site (drainage area of 10 km^2) erosion was deeper and the age of the top of the lower loess is 52 ± 3 ka.

Substantial sediment production from bedrock during the last glacial is known from the Negev (Clapp et al., 2000; Enzel et al., 2012). Today bedrock is exposed on the slopes however the gravel unit may represent the colluvium that was produced during the glacial period. The angular shape of the gravels and their similarity to the surrounding bedrocks suggest that they are the colluvium that had been reworked from the slopes. The high OD values of the OSL samples from this unit (Table 3) indicate partial bleaching, possibly due to short transport distance by flash floods.

Similar gravel units were described at other sites in the Negev Highlands (Fig. 1; Avni et al., 2006, 2012). In places the gravel overlies fluvial loess that was dated to 71–41 ka. That gravel unit was OSL-dated there to 32–17 ka, somewhat older than the ages presented from our study areas. Unlike the small aliquots and single grain measurements used in the current study, those OSL ages were obtained using large aliquots of 5–8 mm which may have contained a mixture of old and young grains that caused age overestimation.

4.1.2.3. Upper loess unit. This unit caps both the Mid- and Late Pleistocene terraces (NZT1, NLZ1, NLZ2, NAR1, NAR2; Figs. 4-6) and its thickness is up to 1 m. The loess was deposited during the early stages of the main incision and was preserved only on relatively high surfaces detached from the newly formed gullies. The age of the unit at the Nizzana and Arod sites is 12–10 ka, whereas at the Loz site, where it is reworked on the slopes, its age is ~5 ka.

Aeolian loess was widely transported and deposited in the Negev Highlands until at least 14 ka (Crouvi et al., 2008). When dust supply to the area diminished, a large reservoir of dust was still available for remobilization by the strong prevailing winds (Roskin et al., 2011a) that redeposited it across the landscape. Even today, entrainment and transport of loess by wind occurs during strong winds in the Negev Highlands, as it did, for example, in the 12/12/2010 storm that was characterized by strong SW winds. This storm formed fresh ripples made of loess aggregates in broad, sandy channels. Notably, the OSL signal of this transported loess was bleached (GSI, unpublished data). Such observations indicate that local reworking of aeolian loess occurs without new supply from external sources.

4.1.3. Holocene terraces

During incision into the middle and late Pleistocene sediments, temporary inset terraces were formed on the banks of the active channels. In the three study sites a low terrace (1–2 m), younger than 0.5 ka, was formed. These low terraces are periodically flooded during heavy floods, and can therefore be easily eroded. The present-day terraces (NZT3, NLZ3 and NZR3) are the latest to form during incision and since incision is still active, these terraces may be entirely eroded in the future and new lower terraces form.

4.2. Aggradation–incision transition

Our results indicate that the transition from aggradation to erosion in the Negev Highlands took place after 28 ka, the youngest age obtained for the lower fluvial loess. Slope erosion that preceded the main incision phase began at 24 ka, early in the LGM. However, the intense incision, as we see it today, started later, around the Pleistocene-Holocene transition (12–10 ka).

Throughout the last glacial period ample loess was deposited, covering the entire landscape, and was subsequently partially washed into the valleys to form the fluvial loess valley-fill. After the LGM, the supply of aeolian loess to the Negev Highlands decreased (Crouvi et al., 2009). As a result, rain started eroding the loess blanket from the slopes and revealed the trapped colluvium. The gradual clearing of the slopes from loess enabled runoff generation with increasing energy (Yair, 1983, 1987; Yair and Kossovsky, 2002). This positive feedback led to colluvium exposure, which could then be transported downslope to the valley. This process is represented by the middle gravel unit dated to 24–8 ka. During that time, aeolian loess was still supplied to the area, however in smaller amounts that did not accumulate on the slopes but were mostly washed further downstream.

While in the northern Negev speleothems were deposited until 13 ka (Vaks et al., 2006), in the Negev Highlands and southern Negev speleothems have not been deposited since 109 ka (Vaks et al., 2010), suggesting aridity similar to that of today in the Negev Highlands and southern Negev. Most studies agree that the LGM in the study area was at least as arid as today (Vaks et al., 2006; Enzel et al., 2008, 2012). There is some evidence for increased rainfall during the latest Pleistocene (10–18 ka uncalibrated ^{14}C) from wood charcoal assemblages from prehistoric sites in the Negev Highlands (Baruch and Goring-Morris, 1997). However, the incision that started at ~12 ka could have begun spontaneously without any increase in precipitation. After the removal of most of the coarse and fine sediment from the slopes and exposure of bedrock, runoff discharge could have generated strong flows in the valleys (Yair and Lavee, 1985) that could easily cut into the sedimentary fill. As incision began, it was intensified by positive feedback. Discharge was channeled in the newly formed gullies, where flow was concentrated and made even more energetic, which amplified incision. This incision is still ongoing (Avni, 2005; Zweig, 2014). Our results support the idea of loess-choked drainage network during the last glacial (Yair and Enzel, 1987; Yair, 1994). Furthermore, we suggest a mechanism for the drainage system to overcome the loess-choked phase.

Nahal Arod drains into the Dead Sea, whose lake levels fluctuated throughout the Late Pleistocene between 170 and 320 m below sea level, with a peak toward the LGM (26 ka; Bartov et al., 2002; Torfstein et al., 2013). At about 14 ka lake levels dropped dramatically and since then have remained at ~400 m below sea level (Torfstein et al., 2013). In contrast, Nahal Nizzana and Nahal Loz drain into the Mediterranean Sea, which reached its lowest level of 115 m below sea level during the LGM (Lambeck and Bard, 2000) and since then has been rising gradually to its current level (Sivan et al., 2001). The different histories of the base levels had no influence on the studied area, since the three studied sites are located very close to the main water divide (Fig. 1) and are 130–150 km distant from their base levels. Local conditions could have also had some influence on the basins' response

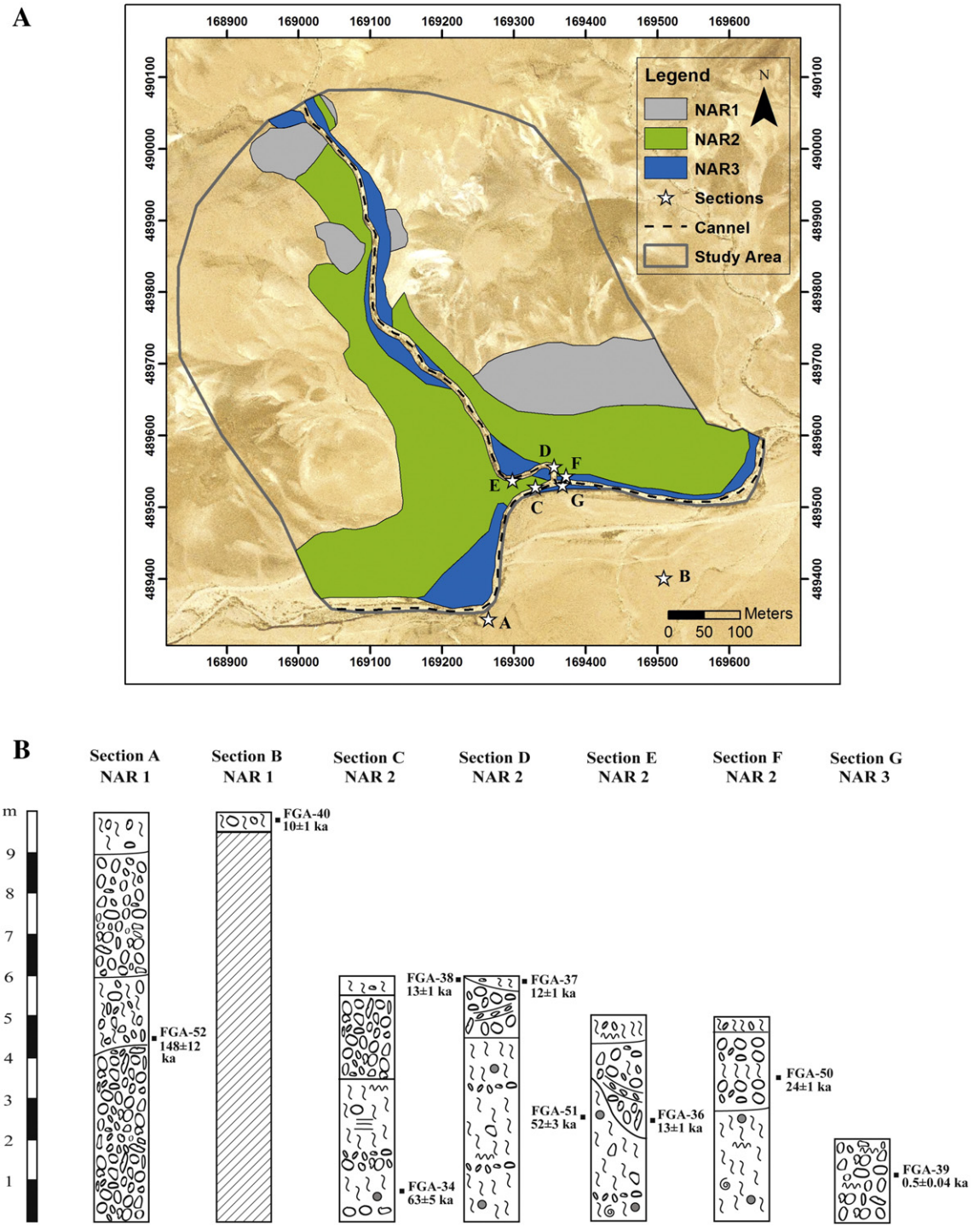

Fig. 6. a. Geomorphological map of Arod site. Stratigraphic sections are marked as stars. b. Stratigraphic sections of Arod site with OSL ages. For legend see Fig. 4b.

to changing climate (Yair and Kossovsky, 2002). For example, the Arod site is located at the eastern termination of loess distribution (Dan and Raz, 1970; Crouvi et al., 2009), possibly with lower loess supply. Or, the Nizzana tributary basin is one order of magnitude smaller than the other two basins (Table 1). Yet, all three studied basins reveal a similar chain of processes, in which fine sediments accumulated on the slopes were washed off the slopes into the valleys, followed by downslope transport of angular local colluvium into the valleys, ending with deep incision. The similar timing indicates a more regional control over the basins' response.

4.3. Regional framework

The Negev Highlands are positioned between central Israel with a Mediterranean climate and the semi-arid northern Negev in the north, and the hyper-arid southern Negev in the south. They form a local orographic obstacle to winter rain-bearing systems coming from the Mediterranean. The NW aspect of the Negev Highlands is the southernmost area that receives regular winter precipitation from the Mediterranean (Enzel et al., 2008). Rare, intense synoptic systems also reach the area from the south. It has been suggested that during the last glacial period,

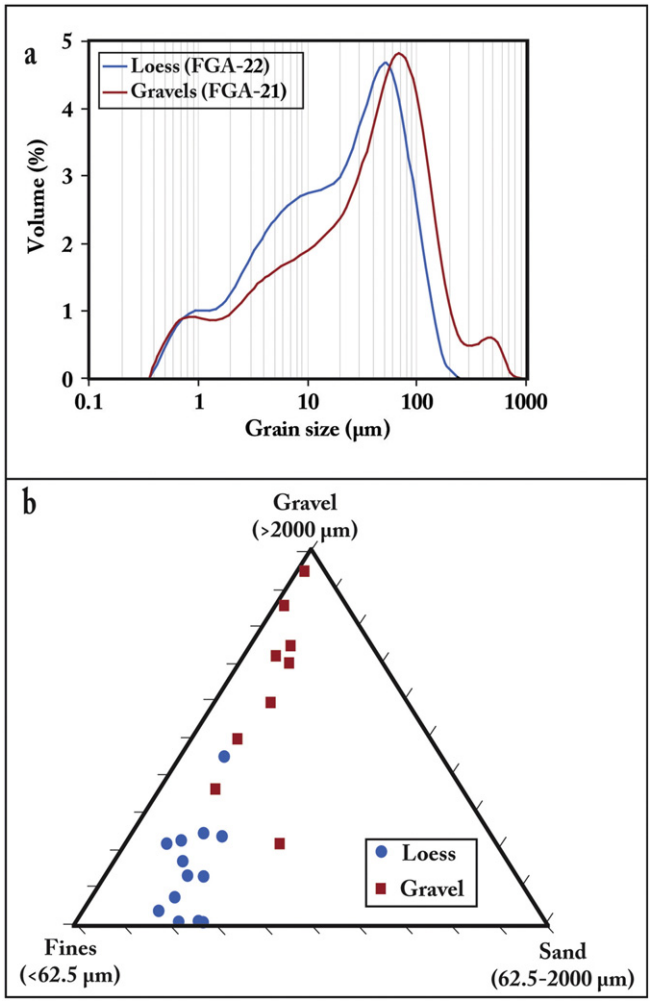

Fig. 7. a. Particle size distribution (<1000 μm) of two representative loess and gravel samples from the Nizzana site. Aside from the small tail of coarse particles in the gravel sample, the two samples are very similar. b. Ternary diagram for all loess and gravel samples showing the percentage of gravels, sand, and fine (silt + clay) particles. Note the low percentage of sand in all samples.

precipitation in the northern Negev and in central Israel may have been up to double that of today (Bartov et al., 2002; Vaks et al., 2006; Enzel et al., 2008; Ryb et al., 2014). However, during LGM, sea level was much lower and the Sinai coastline reached its farthest point ~50 km north of the present-day coast (Enzel et al., 2008). As a result, fewer storms reached the Negev Highlands from the Mediterranean and the amount of rainfall was reduced. This, together with strong winds (Enzel et al., 2010; Roskin et al., 2011a), allowed the accumulation of windblown dust into the thick loess sections covering valley floor and slope colluvium.

Unlike the Negev Highlands, the southern Negev has been hyperarid at least since the middle Pleistocene (Amit et al., 2006, 2011; Matmon et al., 2009; Vaks et al., 2010; Enzel et al., 2012). It also never experienced significant dust supply as the Negev Highlands (Yaalon and Dan, 1974). Nahal Yael (Fig. 1), a small catchment (0.5 km^2) incising through basement rocks in the Eilat Mountains, experienced increased sediment production during the last glacial (Enzel et al., 2012). Slope sediments in this basin were produced mainly at 35–20 ka, during more frequent rain events causing cycles of wetting and drying in the presence of salts that triggered bedrock shattering. This caused intensified rock disintegration and sediment production. The rock fragments were deposited on the slopes, in stream terraces, and on the alluvial fan at the outlet of the basin. Sediment deposition in the stream bed, simultaneous with its production on the slopes, was caused by local runoff discharge that was possible due to the absence of dust cover. This is in contrast to the Negev Highlands, where the produced sediment/regolith on the slopes could reach the valley only after the removal of the loess.

Active incision in Nahal Yael and the nearby Nahal Mekorot started immediately after the LGM, at 20–18 ka (Amit et al., 2007; Enzel et al., 2012), prior to the Negev Highlands. Similar ages of initial incision are known also from the hyperarid areas on eastern side of the Dead Sea rift, at Wadi Sabra, Jordan (Bertrams et al., 2012). There, incision was dated to 18 ka following sedimentation of fluvial and aeolian-fluvial sediments since 38 ka. Thus, in the absence of slope mantling dust, incision was initiated there several thousands of years before it began in the loess-choked basins of the Negev Highlands.

Between the LGM and the Holocene, significant climatic changes occurred in the Levant. These are recorded in the fluctuations of Lake Lisan levels (Bartov et al., 2002; Torfstein et al., 2013), stalactite and stalagmite growth rates (Vaks et al., 2006), dune mobilization and stabilization (Roskin et al., 2011b), and rates of loess supply (Crouvi et al., 2008). The loess covering the central and northern Negev indicates a regime of strong winds during the last glacial lasting up to 14 ka (Crouvi et al., 2008; Enzel et al., 2008). Similarly, dune stabilization ages in the NW Negev support strong winds at least from the LGM to 10 ka (Roskin et al., 2011b). The significant reduction in wind intensity by 10 ka substantially reduced dust supply within the region and allowed initiation of intense incision that began at about that time.

4.4. Global correlations

In many arid and semi-arid regions around the world, increased dust transport was possible during the late Pleistocene due to strong global wind patterns (McGee et al., 2010). Aeolian sediments were deposited as sand dunes and desert loess (Crouvi et al., 2010; Lomax et al., 2011; Telfer, 2011), and later washed and redeposited in fluvial systems. In many places, incision into the redeposited fluvial sediments characterizes the Holocene (e.g. Waters and Haynes, 2001; Avni et al., 2010; Walker and Fattahi, 2011). Although incision at the glacial–interglacial transition is known in arid and semi-arid regions of the world, different reasons triggered incision in the different regions. In Namibia, for example, incision within fine fluvial sediments started at the latest Pleistocene–early Holocene as a result of increased precipitations (Eitel et al., 2001, 2006). The incision in alluvial fans at different sites in eastern Iran started at ~9 ka. It is attributed to decrease in sediment supply and increase in precipitation during the early–middle Holocene (Walker and Fattahi, 2011). At the Gobi Desert margins, Chifeng region, Inner Mongolia, fine loess, which was the main sediment deposited during the last glacial, was incised by small tributaries along the main valley during the Holocene (Avni et al., 2010). During the same time in the Mu Us Desert at the center of Inner Mongolia, incision began only at 2 ka, when the summer monsoon weakened (Li et al., 2012).

The Negev Highlands and the Flinders Ranges, South Australia (Williams et al., 2001; Haberlah et al., 2010) show great similarities in sediment characteristics, chain of events and chronology. In the Flinders Ranges a large amount of aeolian loess was deposited during the last glacial, covering the landscape including valley slopes. The loess was washed from the slopes and redeposited in the valleys, accumulating sections of up to 18 m thick. The dust originated from exposed playa surfaces and nearby dune fields. When dust supply decreased, the loess was washed from the slopes and the buried colluvium was exposed. The colluvium was washed during floods and redeposited in the valleys. Colluvium redeposition started in some places at 24 ka, while in other valleys loess deposition continued up to 18 ka, although at lower rates. Eighteen thousand years ago incision began simultaneously in many streams in the region. Haberlah et al. (2010) attributed the beginning of the incision to a decrease in dust supply, caused by an increase in summer rains which flooded the playas.

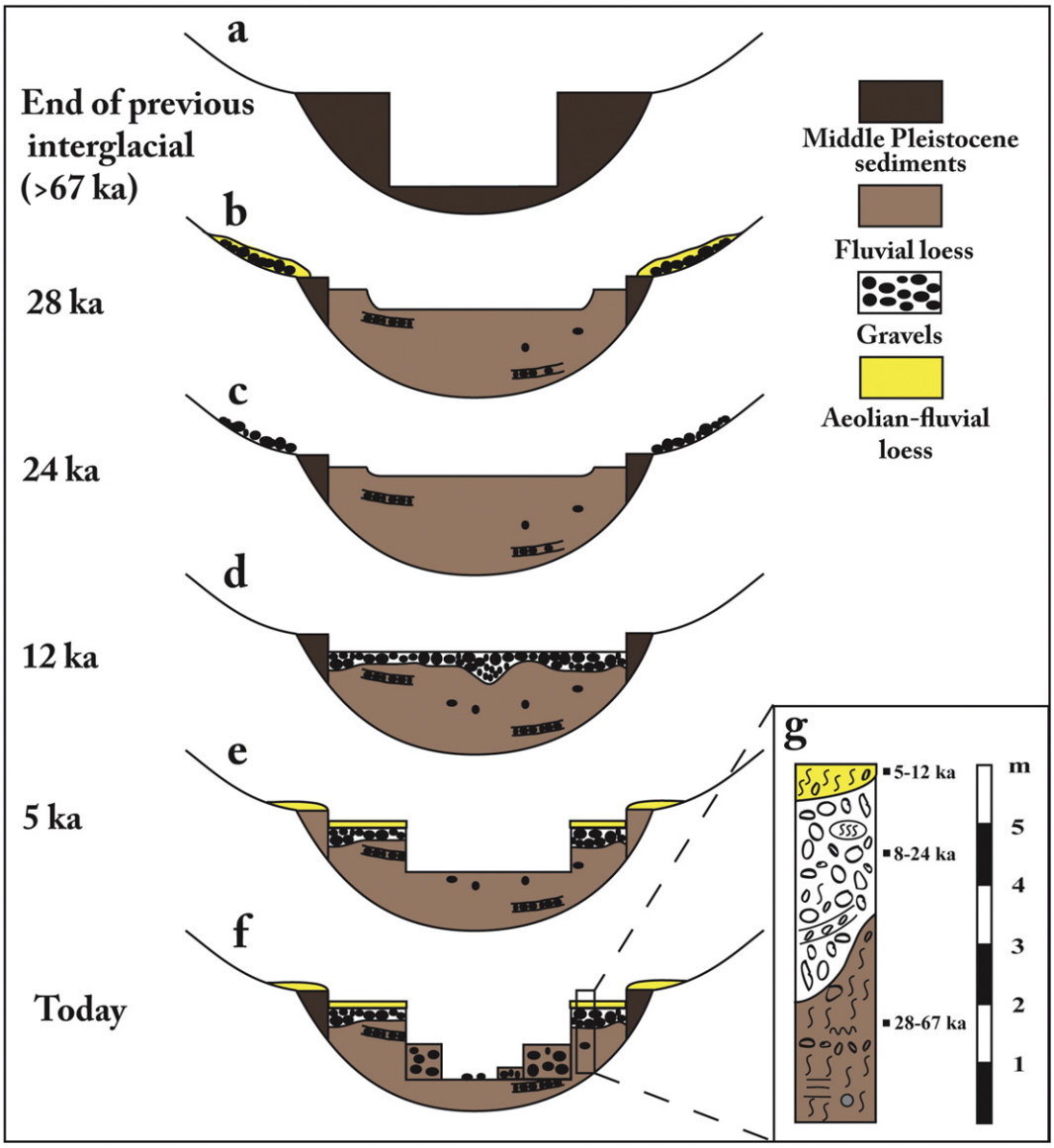

Fig. 8. Schematic cross-sections of a valley fill in the Negev Highland showing snapshots in time of the main geomorphological steps from the late Pleistocene until today. By the end of the last interglacial, valleys were deeply cut into sediments that were deposited probably during the penultimate glacial cycle (a). During the last glacial, ample loess was deposited, covering valleys and slopes (b). At 28–24 ka, aeolian–loess supply decreased and the loess cover was washed from the slopes, revealing the trapped colluvium (c). At 24 ka erosion was initiated with the redeposition of slope colluvium as gravels within the valley, while eroding the underlying sediment (d). At 12 ka incision began with cutting of deep gullies. At the same time aeolian–fluvial loess was deposited, continuing up to 5 ka (e). During incision low terraces were deposited and eroded (f). Incision has been ongoing since then and even intensifying. A representative columnar section of the main terrace at the three study areas is shown in (g).

The similarity between the Negev Highland and the Flinders Ranges, two regions from different hemisphere, is the result of similar environmental conditions. In both areas large amounts of wind-blown dust choked the drainage systems. The gullies could incise through the valley-fill only when dust supply dropped. In the Negev it happened when global winds weakened at the transition to the Holocene, while in the Flinders Ranges it happened when the dust source was flooded following increased precipitation.

5. Conclusions

Sedimentary fill sections were studied at three small catchments in the Negev Highlands, southern Israel. Our results show that the main, late Pleistocene terrace in all three study sites is composed of similar units with similar OSL ages, although the basins vary in size and drain to different base levels. The units are: A lower fluvial loess unit (67–28 ka), a middle gravel unit, which truncates the lower loess (24–8 ka), and an upper loess unit of aeolian–fluvial origin (12–5 ka). This indicates that in our case base level does not control the timing of aggradation or incision but mainly regional environmental and climate conditions. The loess cover that choked the drainage system during the last glacial inhibited erosion and incision until reduction in dust supply and removal of the loess blanket from the slopes.

The temporal framework for the evolution of the Negev Highlands modern landscape is constructed as follows (Fig. 8):

- By the end of the last interglacial erosion created accommodation space in the stream channels and only patchy older terraces remained.
- Fluvial loess was extensively deposited on the slopes and in the valleys since at least 67 ka until after 28 ka.
- Decrease in aeolian loess supply initiated the erosion of fine and coarse sediment from the slopes into the channels at 28–24 ka.

- Gravel units originating as colluvium on the slopes were deposited at 24–8 ka, incising into the upper part of the underlying fluvial loess unit.
- As bedrock was exposed on the slopes, runoff discharge increased and major incision began at 12 ka forming deep and relatively narrow gullies.
- Incision has been ongoing since 12 ka and has intensified through positive feedback of concentration of runoff discharge into narrow channels, increasing incision power.
- The upper loess was deposited and reworked at ~12–5 ka and was preserved only on relatively high surfaces detached from the newly formed gullies.
- During incision temporary low terraces are being deposited and eroded. The current cycle of those temporary terraces is <0.5 ka.

Acknowledgments

The research was funded by the Earth Science Research Administration of the Israel Ministry of Energy and Water Resources in Jerusalem, grant number 29-17-051. We thank Y. Rephael, Y. Mizrachi and I. Swaed for assistance in fieldwork, Z. Dolgin for help in sample preparation, D. Stuber and O. Yoffe for chemical analyses and M. Ben-Israel and R. Krasilshikov for PSD analysis. We thank two anonymous reviewers for their insightful comments that improved this manuscript.

Appendix A. Supplementary data

Supplementary data to this article can be found online at http://dx.doi.org/10.1016/j.geomorph.2015.10.017.

References

Amit, R., Enzel, Y., Sharon, D., 2006. Permanent Quaternary aridity in the southern Negev, Israel. Geology 34, 509–512.
Amit, R., Lekach, J., Ayalon, A., Porat, N., Grodek, T., 2007. New insight into pedogenic processes in extremely arid environments and their paleoclimatic implications—the Negev Desert, Israel. Quat. Int. 162–163, 61–75.
Amit, R., Enzel, Y., Crouvi, O., Simhai, O., Matmon, A., Porat, N., McDonald, E., Gillespie, A.R., 2011. The role of the Nile in initiating a massive dust influx to the Negev late in the middle Pleistocene. Geol. Soc. Am. Bull. 123, 873–889.
Arnold, L.J., Roberts, R.G., 2009. Stochastic modeling of multi-grain equivalent dose (De) distributions: implications for OSL dating of sediment mixtures. Quat. Geochronol. 4, 204–230.
Avni,Y., 1991. The geology, paleogeography and the landscape evolution of the central Negev Highlands and the western Ramon structure. Geological Survey of Israel, GSI/6/91, (in Hebrew, English abstract).
Avni, Y., 2005. Gully incision as a key factor in desertification in an arid environment, the Negev Highlands, Israel. Catena 63, 185–220.
Avni, Y., Porat, N., Plakht, J., Avni, G., 2006. Geomorphologic changes leading to natural desertification processes versus anthropogenic land conservation in an arid environment, the Negev Highlands, Israel. Geomorphology 82, 177–200.
Avni, Y., Zhang, J., Shelah, G., Zioao, L., 2010. Upper Pleistocene-Holocene geomorphic changes dictating sedimentation rates and historical land use in the valley system of the Chifeng region, Inner Mongolia, northern China. Earth Surf. Process. Landf. 35, 1251–1268.
Avni, Y., Porat, N., Avni, G., 2012. Pre-farming environment and OSL chronology in the Negev Highlands, Israel. J. Arid Environ. 86, 12–27.
Bartov, Y., Stein, M., Enzel, Y., Agnon, A., Reches, Z., 2002. Lake levels and sequence stratigraphy of Lake Lisan, the late Pleistocene precursor of the Dead Sea. Quat. Res. 57, 9–21.
Baruch, U., Goring-Morris, A.N., 1997. The arboreal vegetation of the Central Negev Highlands, Israel, at the end of the Pleistocene; evidence from archaeological charred wood remains. Vegetation History and Archaeobotany 6, 249–259.
Ben-David, R., 2003. Changes in Desert Margin Environments During the Climate Changes of the Late Quaternary: Interaction Between Drainage Systems and the Accumulation of Dust (Loess) and the Invasion of Dunes at the North-west Negev Desert (Ph.D thesis) Hebrew University of Jerusalem, Jerusalem (in Hebrew, English abstract).
Bertrams, M., Protze, J., Löhrer, R., Schyle, D., Richter, J., Hilgers, A., Klasen, N., Schmidt, C., Lehmkuhl, F., 2012. Multiple environmental change at the time of the Modern Human passage through the Middle East: first results from geoarcheological investigations on Upper Pleistocene sediments in the Wadi Sabra (Jordan). Quat. Int. 274, 55–72.
Botha, G.A., Wintle, A.G., Vogel, J.C., 1994. Episodic late Quaternary paleogully erosion in northern KwaZulu-Natal, South Africa. Catena 23, 337–340.
Bøtter-Jensen, L., Murray, A.S., 1999. Developments in optically stimulated luminescence techniques for dating and retrospective dosimetry. Radiat. Prot. Dosim. 84, 307–315.
Bøtter-Jensen, L., Buler, E., Duller, G.A.T., Murray, A.S., 2000. Advances in luminescence instrument systems. Radiat. Meas. 32, 523–528.
Bowman, D., Karnieli, A., Issar, A., Bruins, H.J., 1986. Residual colluvio-aeolian aprons in the Negev Highlands (Israel) as a paleo-climatic indicator. Palaeogeogr. Palaeoclimatol. Palaeoecol. 56, 89–101.
Bruins, H.J., Yaalon, D.H., 1979. Stratigraphy of the Netivot section in the desert loess of the Negev (Israel). Acta Geol. Acad. Sci. Hung. 22, 161–169.
Bull, B.B., 1997. Discontinuous ephemeral streams. Geomorphology 19, 227–276.
Clapp, E.M., Bierman, P.R., Schick, A.P., Lekach, J., Enzel, Y., Caffee, M., 2000. Differing rates of sediment productions and sediment yield determined by cosmogenic isotopes and conventional methods in extremely arid environment, Nahal Yael, Israel. Geology 28, 995–998.
Clarke, M.L., Vogal, J.C., Botha, G.A., Wintle, A.G., 2003. Late Quaternary hillslope evolution recorded in eastern South Africa colluvial badlands. Palaeogeogr. Palaeoclimatol. Palaeoecol. 197, 199–212.
Crouvi, O., Amit, R., Enzel, Y., Porat, N., Sandler, A., 2008. Sand dunes as a major proximal dust source for late Pleistocene loess in the Negev desert, Israel. Quat. Res. 70, 275–282.
Crouvi, O., Amit, R., Porat, N., Gillespie, A.R., McDonald, E.V., Enzel, E., 2009. Significance of primary hill top loess in reconstructing dust chronology, accretion rates, and sources: an example from the Negev desert. Israel. Journal of Geophysical Research 114.
Crouvi, O., Amit, R., Enzel, Y., Gillespie, A.R., 2010. Active sand seas and the formation of desert loess. Quat. Sci. Rev. 29, 2087–2098.
Dan, J., Raz, Z., 1970. The Soil Association Map of Israel. Volcani Institute, Bet Dagan, Israel.
Davidovich, U., Porat, N., Gadot, Y., Avni, Y., Lipschits, O., 2012. Archaeological investigations and OSL dating of terraces at Ramat Rahel, Israel. Journal of Field Archaeology 37, 192–208.
Duller, G.A.T., 2003. Distinguishing quartz and feldspar in single grain luminescence measurements. Radiat. Meas. 37, 161–165.
Eitel, B., Blumel, W.D., Huser, K., Mouz, B., 2001. Dust and loessic alluvial deposits in northwestern Namibia (Damaraland, Kaokoveld): sedimentology and paleoclimatic evidence based on luminescence data. Quat. Int. 76 (77), 57–65.
Eitel, B., Kadereit, A., Blumel, W.D., Huser, K., Lomax, J., Hilgers, A., 2006. Environmental changes at the eastern Namib desert margin before and after the last glacial maximum: new evidence from fluvial deposits in the upper Hoanib River catchment, northwestern Namibia. Palaeogeogr. Palaeoclimatol. Palaeoecol. 234, 201–222.
Enzel, Y., Amit, R., Dayan, U., Crouvi, O., Kahana, R., Ziv, B., Sharon, D., 2008. The climatic and physiographic controls of the eastern Mediterranean over the Late Pleistocene climates in the southern Levant and its neighboring deserts. Glob. Planet. Chang. 60, 165–192.
Enzel, Y., Amit, R., Crouvi, O., Porat, N., 2010. Abrasion-derived sediments under intensified winds at the latest Pleistocene leading edge of the advancing Sinai-Negev erg. Quat. Res. 74, 121–131.
Enzel, Y., Amit, R., Drodek, T., Ayalon, A., Lekach, J., Porat, N., Bierman, P., Blum, J.D., Erel, Y., 2012. Late Quaternary weathering, erosion, and deposition in Nahal Yael, Israel: an "impact of climatic change on an arid watershed"? GSA Bull. 124, 705–722.
Eshel, G., Levy, G.J., Mingrlgrin, U., Singer, M.J., 2004. Critical evaluation of the use of laser diffraction for particle-size distribution analysis. Soil Sci. Soc. Am. J. 68, 736–743.
Galbraith, R.F., Roberts, R.G., 2012. Statistical aspects of equivalent dose and error calculation and display in OSL dating: an overview and some recommendations. Quat. Geochronol. 11, 1–27.
Gerson, R., Amit, R., 1987. Rates and modes of dust accretion and deposition in an arid region—the Negev, Israel. Geol. Soc. Lond., Spec. Publ. 35, 157–169.
Goodfriend, G.A., Magaritz, M., 1988. Palaeosols and late Pleistocene rainfall fluctuations in the Negev desert. Nature 332, 144–146.
Haberlah, D., Williams, M.A.J., Halverson, G., McTainsh, G.H., Hill, S.M., Hrstka, T., Jaime, P., Butcher, A.R., Glasby, P., 2010. Loess and floods: high-resolution multi-proxy data of Last Glacial Maximum (LGM) slackwater deposition in the Flinders Ranges, semi arid South Australia. Quat. Sci. Rev. 29, 2673–2693.
Hall, J., 1997. Digital Shaded-Relief Map of Israel and Environs, 1:500000. Israel Geological Survey.
Horowitz, A., 1979. The Quaternary of Israel. New York Academic Press.
Issar, A.S., Bruins, H.J., 1983. Special climatological conditions in the deserts of Sinai and the Negev during the latest Pleistocene. Palaeogeogr. Palaeoclimatol. Palaeoecol. 43, 63–72.
Jacobs, Z., Wintle, A.G., Roberts, R.G., Duller, G.A.T., 2008. Equivalent dose distributions from single grains of quartz at Sibudu, South Africa: context, cause and consequences for optical dating of archaeological deposits. J. Archaeol. Sci. 35, 1808–1820.
Kahana, R., Ziv, B., Enzel, Y., Dayan, U., 2002. Synoptic climatology of major floods in the Negev desert, Israel. Int. J. Climatol. 22, 867–882.
Lambeck, K., Bard, E., 2000. Sea-level change along the French Mediterranean coast for the past 30 000 years. Earth Planet. Sci. Lett. 175, 203–222.
Li, S.H., Sun, J., Li, B., 2012. Holocene environmental changes in central Inner Mongolia revealed by luminescence dating of sediments from the Sala Us River valley. The Holocene 22, 397–404.
Lomax, J., Hilgers, A., Radtke, U., 2011. Palaeoenvironmental change recorded in the palaeodunefields of the western Murray Basin, South Australia: new data from single grain OSL-dating. Quat. Sci. Rev. 30, 723–736.
Magaritz, M., 1986. Environmental changes records in the Upper Pleistocene along the desert boundary, southern Israel. Palaeogeogr. Palaeoclimatol. Palaeoecol. 53, 9–16.
Matmon, A., Simhai, O., Amit, R., Haviv, I., Porat, N., McDonald, E., Benedetti, L., Finkel, R., 2009. Where erosion ceases: desert pavement coated surfaces in extreme deserts present the longest-lived landforms on Earth. Geol. Soc. Am. Bull. 121, 688–697.

Mayya, Y.S., Morthekai, P., Murari, M.K., Singhvi, A.K., 2006. Towards quantifying beta microdosimetric effects in single-grain quartz dose distribution. Radiat. Meas. 41, 1032–1039.
McGee, D., Broecker, W.S., Winckler, G., 2010. Gustiness: the driver of glacial gustiness? Quat. Sci. Rev. 29, 2340–2350.
Medialdea, A., Thomsen, K.J., Murray, A.S., Benito, G., 2014. Reliability of equivalent-dose determination and age-models in the OSL dating of historical and paleofloods sediments. Quat. Geochronol. 22, 11–24.
Mix, A.C., Bard, E., Schneider, R., 2001. Environmental processes of the ice age: land, oceans, glaciers (EPILOG). Quat. Sci. Rev. 20, 627–657.
Murray, A.S., Wintle, A.G., 2000. Luminescence dating of quartz using an improved single-aliquot regenerative-dose protocol. Radiat. Meas. 32, 57–73.
Olley, J.M., Pietsch, T., Roberts, R.G., 2004. Optical dating of Holocene sediments from a variety of geomorphic settings using single grains of quartz. Geomorphology 60, 337–358.
Porat, N., 2006. Use of magnetic separation for purifying quartz for luminescence dating. Ancient TL 24, 33–36.
Porat, N., Duller, G.A.D., Amit, R., Zilberman, E., Enzel. Y., 2009. Recent faulting in the southern Arava, Dead Sea Transform: evidence from single grain luminescence dating. Quat. Int. 199, 34–44.
Porat, N., Faerstein, G., Medialdea, A., Murray, A.S., 2015. Re-examination of common extraction and purification methods of quartz and feldspar for luminescence dating. Ancient TL 33, 22–30.
Roberts, R.G., Galbraith, R.F., Yoshida, H., Laslett, G.M., Olley, J.M., 2000. Distinguishing dose populations in sediment mixtures: a test of single-grain optical dating procedures using mixture of laboratory-doses quartz. Radiat. Meas. 32, 459–465.
Roberts, H.M., Duller, G.A.T., 2004. Standardised growth curves for optical dating of sediment using multiple-grain aliquots. Radiat. Meas. 38, 241–252.
Rodnight, H., Duller, G.A.T., Wintle, A.G., Tooth, S., 2006. Assessing the reproducibility and accuracy of optical dating of fluvial deposits. Quat. Geochronol. 1, 119–120.
Roskin, J., Tsoar, H., Porat, N., Blumberg, D.G., 2011a. Palaeoclimate interpretations of Late Pleistocene vegetated linear dune mobilization episodes: evidence from the northwestern Negev dunefield, Israel. Quat. Sci. Rev. 33, 3364–3380.
Roskin, J., Porat, N., Tsoar, H., Blumberg, D.G., Zander, A.M., 2011b. Age, origin and climatic control on vegetated linear dunes in the northwestern Negev desert (Israel). Quat. Sci. Rev. 30, 1649–1674.
Russell, N.J., Armitage, S.J., 2012. A comparison of single-grain and small aliquot dating of fine sand from Cyrenaica, northern Libya. Quat. Geochronol. 10, 62–67.
Ryb, U., Matmon, A., Erel, Y., Haviv, I., Katz, A., Starinsky, A., Angert, A., ASTER Team, 2014. Controls on denudation rates in tectonically stable Mediterranean carbonate terrain. Geol. Soc. Am. Bull. 126, 553–568.
Sharon, D., 1972. The spottiness of rainfall in desert areas. J. Hydrol. 17, 161–175.
Sharon, D., Kutiel, H., 1986. The distribution of rainfall intensity in Israel, its regional and seasonal variations and its climatological evaluation. J. Hydrol. 6, 277–291.
Sivan, D., Wdowinski, S., Lambeck, K., Galili, E., Raban, A., 2001. Holocene sea-level changes along the Mediterranean coast of Israel, based on archaeological observations and numerical model. Palaeogeogr. Palaeoclimatol. Palaeoecol. 167, 101–117.
Telfer, M.W., 2011. Growth by extension, and reworking, of a south-western Kalahari inear dune. Earth Surf. Process. Landf. 36, 1125–1135.
Thomsen, K.J., Bøtter-Jensen, L., Denby, P.M., Moska, P., Murray, A.S., 2006. Development in luminescence measurements techniques. Radiat. Meas. 41, 768–773.
Torfstein, A., Goldstein, S.L., Stein, M., Enzel, Y., 2013. Impacts of abrupt climate changes in the Levant from Last Glacial Dead Sea levels. Quat. Sci. Rev. 69, 1–7.
Tsvieli, Y., Zangvil, A., 2007. Synoptic climatological analysis of Red Sea Trough and non-Red Sea Trough rain situations over Israel. Adv. Geosci. 12, 137–143.
Vaks, A., Bar-Matthews, M., Ayalon, A., Matthews, A., Frumkin, A., Dayan, U., Halicz, L., Almogi-Labin, A., Schilman, B., 2006. Palaeoclimate and location of border between Mediterranean climate region and the Saharo–Arabian desert as revealed by speleothems from the northern Negev desert, Israel. Earth Planet. Sci. Lett. 249, 384–399.
Vaks, A., Bar-Matthews, M., Matthews, A., Ayalon, A., Frumkin, A., 2010. Middle-Late Quaternary paleoclimate of northern margins of the Saharan–Arabian desert: reconstruction from speleothems of Negev desert, Israel. Quat. Sci. Rev. 29, 2647–2662.
Walker, R.T., Fattahi, M., 2011. A framework of Holocene and Late Pleistocene environmental change in eastern Iran inferred from the dating of periods of alluvial fan abandonment, river terracing, and lake deposition. Quat. Sci. Rev. 30, 1256–1271.
Waters, M.R., 1988. Holocene alluvial geology and geoarchaeology of the San Xavier reach of the Santa Cruz river, Arizona. Geol. Soc. Am. Bull. 100, 479–491.
Waters, M.R., Haynes, C.V., 2001. Late Quaternary arroyo formation and climate change in the American southwest. Geology 29, 399–402.
Williams, M.A.J., Prescott, J.R., Chappell, J., Adamson, D., Cock, B., Walker, K., Gell, P., 2001. The enigma of a late Pleistocene wetland in the Flinders Ranges, South Australia. Quat. Int. 83-85, 129–144.
Yaalon, D., Dan, J., 1974. Accumulation and distribution of loess-derived deposits in the semi-desert and desert fringe areas of Israel. Zeitschrift für Geomorphologie NF 20, 91–105.
Yair, A., 1983. Hillslope hydrology, water harvesting and areal distribution of some ancient agricultural systems in the northern Negev desert. J. Arid Environ. 6, 163–184.
Yair, A., 1987. Environmental effects of loess penetration into the northern Negev desert. J. Arid Environ. 13, 9–14.
Yair, A., 1994. The ambiguous impact of climate change at a desert fringe: northern Negev, Israel. In: Millington, A.C., Pye, K. (Eds.), Environmental Change in Drylands: Biogeographical and Geomorphological Perspectives. Wiley, Chichester, pp. 199–227.
Yair, A., Lavee, H., 1985. Runoff generation in arid and semi-arid areas. In: Anderson, M.G., Burt, T.P. (Eds.), Hydrological Forecasting. Wiley, Chichester, pp. 183–220.
Yair, A., Enzel, Y., 1987. The relationship between annual rainfall and sediment yield in arid and semi-arid areas. The case of the northern Negev. Catena Suppl. 10, 121–135.
Yair, A., Kossovsky, A., 2002. Climate and surface properties: hydrological response of small arid and semi-arid watersheds. Geomorphology 42, 43–57.
Zilberman, E., 1991. Landscape Evolution in the Central, northern and northwestern Negev during the Neogene and the Quaternary. Geological Survey of Israel, GSI/45/90, (in Hebrew, English abstract).
Zilberman, E., 1993. The Late Pleistocene sequence of the northwestern Negev flood plains — a key to reconstructing the paleoclimate of southern Israel in the last glacial. Isr. J. Earth Sci. 41, 155–168.
Zweig, R.L., 2014. Quantification and modeling of land degradation processes in arid environments using terrestrial laser scanning (M.Sc. thesis) The Technion 98 pp.